Journal of Statistical Physics, Vol. 82, Nos. 3/4, 1996

Monte Carlo Studies of a Driven Lattice Gas. I. Growth and Asymmetry During Phase Segregation

F. J. Alexander,[1] C. A. Laberge,[2] J. L. Lebowitz,[2] and R. K. P. Zia[3]

Received February 6, 1995; final July 6, 1995

We investigate the effects of an external field on the kinetics of phase segregation in systems with conservative diffusive dynamics. We find that, in contrast to the situation without a field, there are now qualitative differences between the results of microscopic simulations of a 2D lattice model with biased Kawasaki exchanges and those obtained from various modifications of the macroscopic Cahn–Hilliard equation (mCH). While both microscopic simulations and numerical solutions of MCH yield triangular domains, we find that in the former the triangles mainly point *opposite* to the field, while in the latter and in new calculations with the mCH they point *along* the field. On the other hand, the rate of growth of the clusters and their final state, bands parallel to the field, are similar. This issue and the question of the mesoscopic behavior of cell dynamical systems is discussed but not resolved.

KEY WORDS: Driven diffusive systems; phase segregation dynamics.

1. INTRODUCTION

The study of phase segregation occurring when a binary mixture is quenched below its critical temperature T_c has a rich experimental, theoretical, and computational history.[2] There is by now a general consensus that in the late stage of the segregation there exists a scaling regime

[1] Institute for Scientific Computing Research L-416, Lawrence Livermore National Laboratory, Livermore, California 94550. Present address: Center for Computational Science, Boston University Boston, Massachusetts 02215. E-mail: fja@conx.bu.edu.

[2] Departments of Physics and Mathematics, Rutgers University, Piscataway, New Jersey 08855-0849. E-mail: laberge@physics.rutgers.edu; lebowitz@math.rutgers.edu.

[3] Center for Stochastic Processes in Science and Engineering and Department of Physics, Virginia Polytechnic Institute and State University, Blacksburg, Virginia 24061-0435. E-mail: rkpzia@vtvm1.cc.vt.edu.

0022-4715/96/0200-1133$09.50/0

where the system is effectively made up of pure phase regions separated by very narrow interfaces. The system can then be characterized by only one length scale $R(t)$, the characteristic length of the phase domains at time t. Thus typical statistical functions of both space and time are expected to depend only on $r/R(t)$ apart from possible overall amplitudes. Such dynamical scaling is indeed observed in the two-point correlation function $G(r, t)$, i.e., $G(r, t) \propto \tilde{g}(r/R(t))$, and in the closely related structure factor, $S(k, t) \propto \tilde{f}(k/k_m(t))$ with k_m the value of k where S is maximum at time t (see, e.g., ref. 3 for experimental data). For late-stage segregation, it is generally accepted that this length scales according to $R(t) \sim t^{\varphi}$, where $\varphi = 1/3$ when the order parameter is conserved and the dynamics is diffusive.[2, 4] A natural question to ask is how this behavior would change if a constant external field (e.g., electric or gravitational) is present during the phase segregation.

We could arrive at the same question starting from another perspective, namely, phase transitions in driven diffusive systems (DDS).[5] A prototype consists of the usual Ising lattice gas, with the particles subjected to an external driving field so that their motion is biased along one of the axes of the lattice. There has been much interest in the steady states of such systems (see ref. 6 for a review). The second-order Ising transition present in the equilibrium system without a field still exists in the stationary nonequilibrium state with a critical temperature T_c which depends on the field strength. Phase segregation will occur when the system is quenched below this temperature, and we thus we have a different motivation for pursuing the same study, i.e., phase segregation dynamics for systems on their way to a nonequilibrium, rather than an equilibrium, steady state.

Theoretical investigations most frequently follow two distinct avenues: computer simulations of a microscopic model and numerical integration of an equation for the continuum macoscopic densities. For phase segregation of binary alloys in the absence of external fields, the former method relies on the Ising lattice gas with Kawasaki spin-exchange dynamics (e.g., refs. 7–9), while the latter exploits the Cahn–Hilliard (CH)[10] equation without noise (e.g., refs. 11 and 12). Another, less common approach uses cell dynamical systems (CDS) introduced in refs. 13–15, which can be considered as a mesoscopic description of the phenomena. Since all these techniques are phenomenological descriptions attempting to capture the essence of phase segregation in real alloys, none is *a priori* better than the other. It is therefore gratifying (and still somewhat surprising) that, while a given technique might turn out to be more efficient in a given situation, they all give very similar results. This suggests (e.g., ref. 15) that there is an underlying renormalization-group structure and a single universality class behind the phenomena of ordinary phase segregation.

For phase segregation in the presence of an external field, much less is known. While gravity is unavoidable on earth-bound experiments, its effects are either too small in the systems of interest or kept small by choosing materials of comparable densities. On the theoretical front, this problem was studied by Kitaharea *et al.*[16] who showed that we cannot just add the field term to the free energy of the usual CH equation. One needs a modification corresponding to a nonconstant mobility[17, 18] to get any effect at all. They also carried out some simulations using CDS. Later, more quantitative studies[1, 19, 20] used modifications of CH (mCH) whose range of validity remains to be studied. Surprisingly, no one has investigated phase separation dynamics of the lattice gas directly. The aim of this paper is to report on simulation studies of the latter and compare them to both old and new studies of mCH. Though similarities are found for the two-point correlations, dramatic differences are discovered for the three-point function, which is a quantitative measure of the particle–hole asymmetry in the driven system.

In the remainder of the paper, we present the microscopic model in Section 2 and the mCH in Section 3. Our findings and comparisons are given in detail in Section 4. Possible reasons for the major discrepancies are discussed in the final section. In a subsequent paper[21] we will focus on the time evolution of certain shapes of droplets in a further effort to probe the differences between the microscopic and macroscopic approaches.

2. THE MICROSCOPIC MODEL

We consider a two-dimensional square lattice with $N = L_x L_y$ sites and periodic boundary conditions in both directions. Each site is labeled by an index $i = 1, ..., N$ and is either occupied by a type A particle ($\eta_i = 1$) or by a type B particle ($\eta_i = 0$). For simplicity we shall refer to A's as particles and to B's as holes. Given a configuration $\eta = (\eta_1, ..., \eta_N)$ with an overall particle density

$$\rho = \frac{1}{N} \sum_{i=1}^{N} \eta_i \tag{1}$$

the system evolves under a particle-conserving stochastic dynamics. The particles are endowed with nearest neighbor attraction, modeled in the usual way through a Hamiltonian

$$H(\boldsymbol{\eta}) = -4J \sum_{\langle i,j \rangle} \eta_i \eta_j \tag{2}$$

with $J>0$. Furthermore, the particles are biased to move in the direction of an external field E. The entire system is coupled to a thermal bath at a given temperature T. To satisfy local detailed balance, we chose a Metropolis algorithm in which the exchange between two randomly chosen nearest neighbor sites a and b occurs with a probability

$$W(a, b) = \mathrm{Min}[1, \exp\{-H(\boldsymbol{\eta}^{a,b}) - H(\boldsymbol{\eta})]/k_B T + E(x_b - x_a)(\eta_b - \eta_a)\}] \quad (3)$$

where $\boldsymbol{\eta}^{a,b}$ is the configuration after the exchange. Note that the external field E is taken to be in the positive x direction here, so that the particles jump preferably to the right.[5] At half-filling ($\rho = 0.5$) and $E = 0$, this system is known to undergo a second-order phase transition at the Onsager critical temperature $T_c = (2.2692...)J/k_B$. For $E \neq 0$, this transition remains second order and occurs at a higher temperature, saturating at about[22, 23] 1.41 T_c for infinite E. Other theoretical and simulational results on this model are reviewed extensively in ref. 6.

To study phase segregation displayed by this model we used the infinite-temperature homogeneous phase as an initial condition: a configuration consisting of ρN particles and $(1-\rho)N$ holes randomly distributed on the lattice. A rapid quench is then simulated by allowing the configuration to evolve according to the rates given in Eq. (3) with $T < T_c$. Unless otherwise specified, the parameters we chose are $L_x = 512$, $L_y = 256$, $\rho = 0.5$ (half filling), and $T = 0.6T_c$, with E ranging from 0.3 to 1.0. The results will be presented in Section 4 and compared to those from numerical integration of macroscopic evolution equations, a brief summary of which is given next.

3. THE MACROSCOPIC MODELS

In this approach, the discrete variables of the microscopic model are replaced by coarse-grained continuous ones. Thus, instead of occupation numbers at discrete sites, one introduces a density field which serves as the conserved order parameter, be it the density of particles in the model described above or the difference of concentrations of A and B atoms in binary alloys. Of course, the overall average density is a constant, so that the system is often described in terms of $\phi(r, t)$, the deviation of the density from this average at the space-time point (r, t).

Before we discuss the various equations proposed for the driven system, let us briefly summarize the case without an external field. The equation of motion for $\phi(r, t)$ takes the general form[10]

$$\frac{\partial \phi}{\partial t} = \nabla \cdot \left(\mathscr{M} \nabla \frac{\delta \mathscr{F}}{\delta \phi} \right) \quad (4)$$

where $\mathscr{F}\{\phi\}$ is the coarse-grained free energy and $\mathscr{M}$ is the mobility, which is generally a function of ϕ. Equation (4) can be obtained from the continuity equation

$$\frac{\partial \phi}{\partial t} = -\nabla \cdot \mathbf{J} \tag{5}$$

under the assumption that the current J obeys Fick's law

$$\mathbf{J} = -\mathscr{M} \nabla \mu \tag{6}$$

with μ being the local chemical potential

$$\mu(r, t) = \frac{\delta \mathscr{F}}{\delta \phi(r, t)} \tag{7}$$

For $\mathscr{F}$ one generally takes the Ginzburg–Landau free energy functional

$$\mathscr{F}_{\mathrm{GL}} = \int d^d r \left(\frac{\xi^2}{2} |\nabla \phi|^2 - \frac{\tau}{2} \phi^2 + \frac{g}{4} \phi^4 \right) \tag{8}$$

where g, ξ, and τ are phenomenological parameters. Note that we have chosen to write the ϕ^2 term with a negative sign, so that uniform and small ϕ's are unstable for positive τ. This choice models the instability of the homogeneous phase when T is below the critical T_c (conversely, τ should be negative if $T > T_c$). A further simplifying assumption is to take $\mathscr{M}$ to be a constant. With a suitable rescaling of ϕ, r, and t depending on the temperature, Eq. (4) can then be rewritten in the dimensionless form

$$\frac{\partial \phi(r, t)}{\partial t} = -\nabla^2 [\phi(r, t) - \phi(r, t)^3 + \nabla^2 \phi(r, t)] \tag{9}$$

This is the Cahn–Hilliard (CH) equation.[10] With or without the addition of noise it provides the framework for many studies of phase segregation. An initial $\phi(r, 0)$ is chosen, typically from a Gaussian distribution with zero mean, small variance, and delta-function correlations. Then, $\phi(r, t)$ is obtained by integrating this equation numerically via some appropriate discretization (see, e.g., refs. 11 and 12). As pointed out in the Introduction, the results so obtained are in remarkably good quantitative agreement with regard to gross features with both experiments on physical systems and Monte Carlo simulations of lattice gases.

We next consider modifications of this equation to take into account the presence of an external field. A variety of models have been proposed recently. The most naive approach, modifying only the free energy, Eq. (8), by

$$\mathscr{F} = \mathscr{F}_{\mathrm{GL}} - \int d^d r\, E\phi(r, t)x \tag{10}$$

and keeping $\mathscr{M}$ independent of ϕ, leads, as pointed out in ref. 16, to precisely the same CH equation (9). On the other hand, this additional term will survive if we restore the $\phi(r, t)$ dependence to the mobility $\mathscr{M}$. A natural choice[16] is to suppose, as suggested by Langer *et al.*[17] (see also ref. 18) in the context of undriven systems, that $\mathscr{M}(\phi) \simeq 1 - \alpha\phi^2$, where α is a function of temperature with $\alpha\Phi^2 \to 1$ from below as the temperature goes to zero and $|\Phi|$ is the average value of ϕ in the segregated phase, equal to one in our units. This leads to

$$\frac{\partial\phi}{\partial t} = \nabla(1 - \alpha\phi^2)\left[\nabla\left(\frac{\delta\mathscr{F}}{\delta\phi}\right)\right] \tag{11}$$

A modified form of Eq. (11), with ϕ replaced by the magnetization m with $|m| \leqslant 1$, $\mathscr{F}_{\mathrm{GL}}$ replaced by a nonlocal functional of m, and $\alpha = 1$, can in fact be derived rigorously, by suitable scaling of space-time, for lattice models with long-range interactions and Kawasaki exchanges.[24] Expanding Eq. (11) and using the form of $\mathscr{F}$ given in (10) above, it can be recast in the dimensionless form

$$\frac{\partial\phi}{\partial t} = \nabla \cdot [(1 - \alpha\phi^2)\,\nabla(-\phi + \phi^3 - \nabla^2\phi)] + \mathbf{E} \cdot \nabla\phi^2 \tag{12}$$

by appropriate rescaling of ϕ, t, and E. When $\alpha\phi^2$ is typically small, the ϕ dependence of $\mathscr{M}$ in the first term on the right side of the equation is presumably unimportant, and it simplifies to

$$\frac{\partial\phi}{\partial t} = -\nabla\{\phi - \phi^3 + \nabla^2\phi\} + \mathbf{E} \cdot \nabla\phi^2 \tag{13}$$

Equation (13) is the simplest modification to the CH equation, and is directly related to the macroscopic models successful in describing the steady-state properties of our driven systems.[6] Detailed numerical work on the solution of (13) has been performed previously.[1]

We note, however, that in the regime we are considering $\alpha\phi^2$ will typically be close to 1, so its neglect in the term not involving E is not *a priori* justified. [This leaves open the question of why the neglect of this term in Eq. (9) does not seem to have any pronounced effect on the decomposition in this temperature regime.] The fact that $(1-\alpha\phi^2)$ can become negative is also problematic since it may lead to unwanted behavior for the term in the CH equation not involving E. We have therefore investigated a modification of Eq. (11) where $(1-\alpha\phi^2)$ is replaced by $[1-\tanh(\lambda\phi^2)]$, which is more in the spirit of the exact equation described after Eq. (11).[24] This corresponds to replacing Eq. (12) by

$$\frac{\partial\phi}{\partial t}=\nabla\cdot[(1-\tanh(\lambda\phi^2)\,\nabla(-\phi+\phi^3-\nabla^2\phi)]+\mathbf{E}\cdot\nabla\tanh(\lambda\phi^2) \quad (14)$$

We picked $\lambda=2$ [the mobility in the bulk where $|\phi|\sim 1$ is greatly reduced in this case since $1-\tanh(2)=0.036$] and found, somewhat to our surprise, that this new equation gives results which are quite similar, except for time scales, to that obtained from Eq. (13). Some qualitative results on this equation will be presented below (see Figs. 7 and 8), but we will do most of our micro–macro comparisons with solutions of Eq. (13).

We will leave for a later study detailed comparisons with ref. 13 and other mCH equations,[19, 20] which all appear to be qualitatively similar to those in ref. 1. We also hope to make comparisons with CDS studies, which may give different results from the mCH in the presence of a field.

We summarize now the results of refs. 1, 19, and 20 and the present work: except at the earliest stages, the growth is highly anisotropic, so that it is necessary to introduce at least two length scales, $R_{||}(t)$ and $R_{\perp}(t)$, associated with the directions parallel and transverse to the field, respectively. The anisotropy has the following main features:

- An almost-linear growth of the clusters with time in the direction of the field, i.e., $R_{||}(t)\sim t^{\varphi_{||}}$ with $\varphi_{||}\sim 0.8$–0.9 in ref. 1 and $\varphi_{||}\sim 1$ in refs. 19 and 20 and the present work.

- A much reduced, and difficult to measure, growth in the direction perpendicular to the field, i.e., $R_{\perp}(t)\sim t^{\varphi_{\perp}}$, with $\varphi_{\perp}\sim 1/4$ in ref. 1, $\varphi_{\perp}<1/3$ in ref. 19, and $\varphi_{\perp}\sim 1/5$ in the present work. No value was reported in ref. 20.

- Poor dynamical scaling; the two-point correlation functions $G(r, t)$ do not collapse to a single curve when the lengths parallel and transverse to the field are rescaled by $R_{||}(t)$ and $R_{\perp}(t)$, especially at large distances. This is observed by all authors.

• Numerical solutions of Eq. (13) show the formation of triangular domains, with the particle-rich clusters pointing *along* the field, i.e., "downstream".[1] Numerical solutions of Eq. (14) done in the present work also show triangles pointing "downstream" (see Fig. 8). In contrast, the microscopic model studied here leads to triangular clusters pointing "upstream" instead.

4. RESULTS OF SIMULATIONS

Most of the Monte Carlo studies of the microscopic model described in Section 2 used essentially infinite E,[6] since the effects of the drive on the steady states were the main focus. In particular, the only previous comments on time evolution[25] were based on observations made with "infinite E" at the very late stages where the clusters take the form of long, narrow stripes parallel to the field. Since the length of those stripes is essentially the same as the size of the system, the information on cluster growth (in the field direction) and asymmetry (with respect to reflection) was lost. On the other hand, in the studies of the macroscopic model, Yeung *et al.*[1] argued that they were in the regime "small E" and early times. In this regime they found highly anisotropic, as well as asymmetric, behavior. Our present study will focus on the relatively early stages of the phase separation. In this regime we found that there are significant differences between small and large values of E, with the crossover being $E \sim 8J/k_B T$. We shall therefore use small drives, with E typically much smaller than $8J/k_B T$. The main conclusions are: (i) the anisotropic growth laws obtained from the two-point correlation functions are consistent with those in refs. 1 and 19, but (ii) the asymmetry of the clusters is *opposite*, i.e., triangular domains tend to point "upstream." As time evolves, the triangles become more and more elongated, so that they span the system and create the stripes described above. At the very late stages, the stripes will merge into a single band, filling a fraction ρ of the volume.

4.1. Power-Law Growth of Clusters

To study the growth of the clusters with time, we need an estimate of their typical size in a given configuration. To do this we can use information contained in the two-point correlation function $G(\mathbf{r}, t)$ or its Fourier transform, the structure factor $S(\mathbf{k}, t)$. Defining the latter by

$$S(\mathbf{k}, t) = \frac{1}{N} \left| \sum_{\mathbf{r}} e^{-i\mathbf{k}\cdot\mathbf{r}} [\eta(\mathbf{r}, t) - \rho] \right|^2 \tag{15}$$

we find for the former

$$G(\mathbf{r}, t) = \frac{1}{N} \sum_{\mathbf{k}} \exp(i\mathbf{k} \cdot \mathbf{r})\, S(\mathbf{r}, t) \tag{16}$$

When $E = 0$, $G(\mathbf{r}, t)$ is isotropic for distances large compared to the lattice spacing and a convenient choice for a characteristic length $R(t)$ is the value

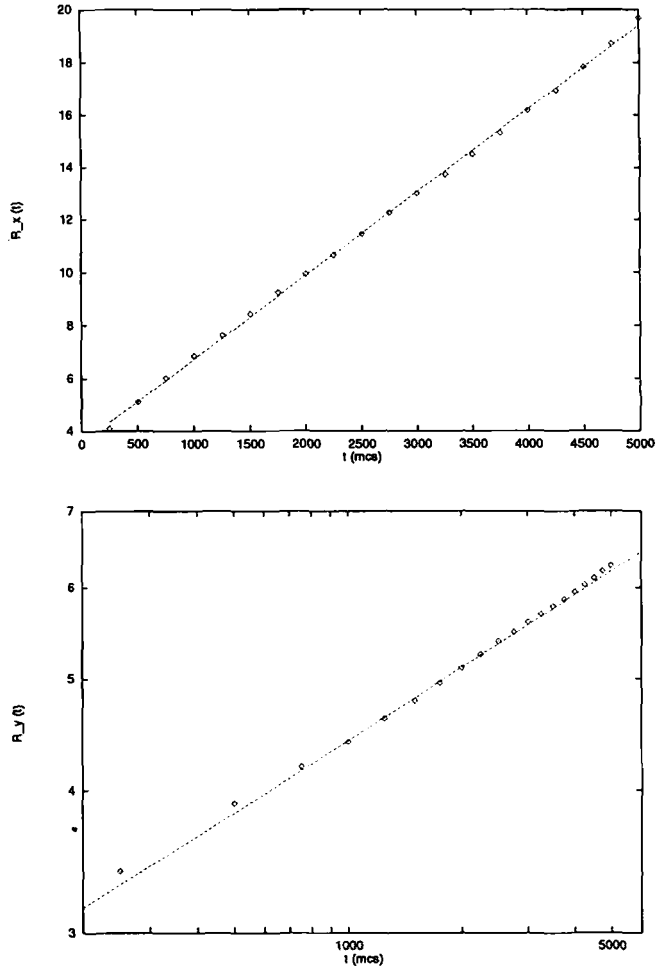

Fig. 1. Plots of $R_x(t)$ and $R_y(t)$ obtained from Monte Carlo simulations. (a) $R_x(t)$ and linear fit, (b) $R_y(t)$ and $t^{0.2}$ on a log–log scale.

of r where $G(r, t)$, the spherical average of $G(\mathbf{r}, t)$, becomes negative for the first time, i.e., $G(R(t), t) = 0$.[26]

In the presence of an external field $\mathbf{E}$ it is natural to introduce the two lengths $R_{||}(t)$ and $R_{\perp}(t)$ via $G(R_x(t), y = 0; t) = 0$ and $G(x = 0, R_y(t); t) = 0$ [We have chosen $\mathbf{E}$ to point in the positive x direction, $(x, y) \equiv (||, \perp)$]. The time dependence of these functions, assumed to be closely related to the actual sizes of the domains, will serve as quantitative measures of cluster growth in these particular directions.

We determined R_x and R_y by using a polynomial of second order to fit the few points of G in the neighborhood of zero and averaged over the results obtained from tend different initial random configurations. Figure 1 shows their behavior in a system of size 512×256 (with $\rho = 0.5$ and $E = 0.5$). Figure 1a strongly suggests that the clusters grow *linearly* with time along the field, i.e.,

$$R_x \sim t^{\varphi_{||}} \qquad \text{with} \quad \varphi_{||} \sim 1 \tag{17}$$

The transversal growth is much slower: a log–log plot of (t) vs. t in Fig. (1b) suggests a power law-behavior of the type

$$R_y \sim t^{\varphi_{\perp}} \qquad \text{with} \quad \varphi_{\perp} \sim 1/5 \tag{18}$$

over the time scale used here. The value of $\varphi_{\perp} \sim 1/5$ should not be taken too seriously, since the range covered is small and later times could well be characterized by a different exponent (in fact it was argued in ref. 1 that $\varphi_{\perp}$ should eventually become 1/3). Nevertheless, this value is consistent with those obtained by numerical integration of the various macroscopic equations.[1, 19]

4.2. Dynamical Scaling

When the system is governed by only one length scale, say $R(t)$, varying with time like $R(t) \sim t^{\varphi}$, then it is reasonable to assume that any function of position and time $F(r, t)$, where F is calculated by averaging over the whole system, may be expressed as $F(r, t) \propto f \sim (r/R(t))$. In other words, apart from a possible overall amplitude, plots of F vs. the scaled variable $r/R(t)$ for various t's will collapse onto one curve: $\tilde{f}$. Such a system is said to display dynamical scaling. In the case of phase segregation without an external field, the radial two-point correlation function $G(r, t)$ collapses once r is rescaled by $R(t)$ as defined after Eq. (16). Likewise the structure factor scales according to $S(k, t) \sim k_m^3 F(k/k_m(t))$,[27, 28] where k_m is the value of k at which S is maximum at time t.

In the highly anisotropic, $E \neq 0$, case, the simplest assumption is that the system is governed by the *two* lengths $R_{||}(t)$ and $R_{\perp}(t)$ defined in Section 4.1. If dynamical scaling is satisfied, then we could expect the correlation functions to collapse, once the appropriate rescaling are performed. Using the same data which gave us Fig. 1 for R_x, R_y, we plot $G(x/R_x(t), 0)/G(0, 0)$ and $G(0, y/R_y(t))/G(0, 0)$ in Fig. 2. The collapse of the functions is quite good near the origin, but this is motly due to the fact that two points (the origin and the position of the first zero of G) are

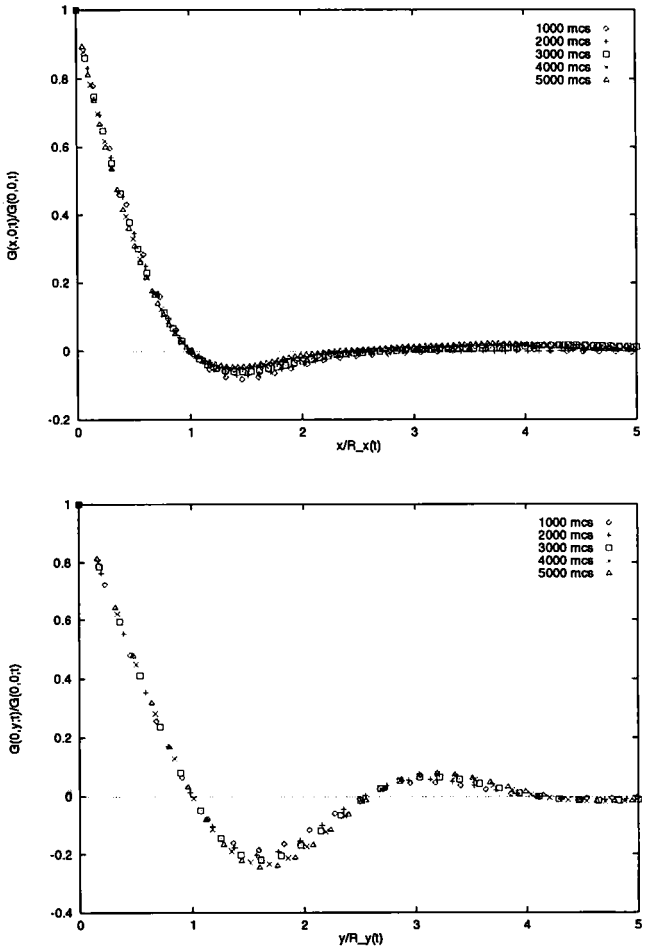

Fig. 2. Dynamical scaling along the x and y directions using data of Fig. 1.

defined to be exactly equal. Beyond the first crossing, the overlap becomes poorer, especially in the direction transverse to the field. Though the lack of collapse appears to remain within reasonable bounds, there is a systematic shift in the data in the sense that the amplitude of oscillation of the rescaled functions is always lower (in x) or higher (in y) for later times. These plots cast serious doubts on the validity of the simple dynamical scaling picture. Alternatively, they suggest that the true scaling regime was not attained in the time scale of our simulations. In Figs. 3–5 we show the

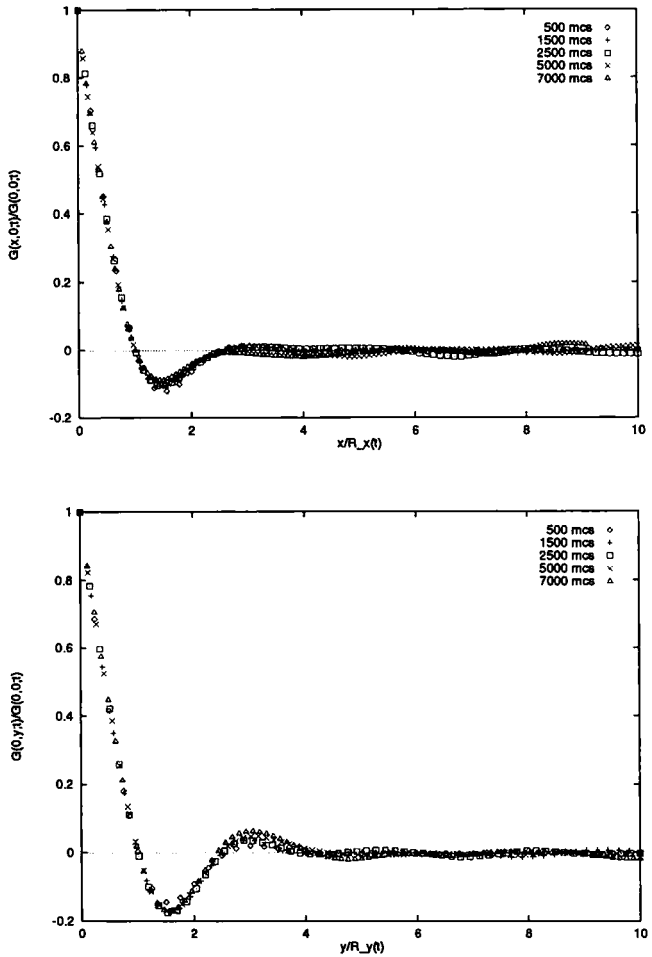

Fig. 3. Dynamical scaling with $E = 0.3$.

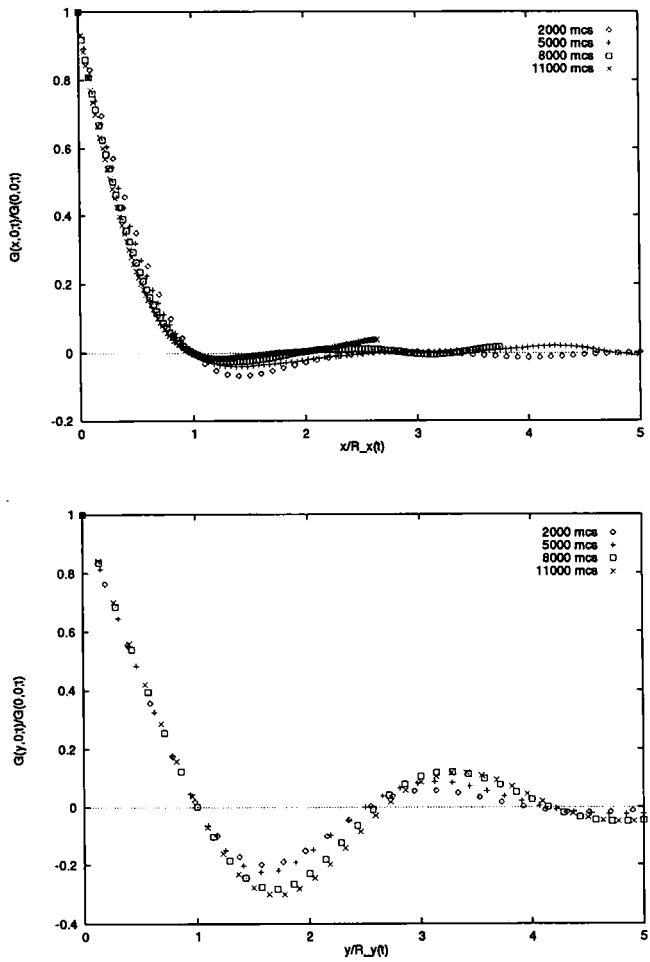

Fig. 4. Dynamical scaling with $E = 0.5$.

data obtained from a single run on a 1024×512 lattice with $\rho = 0.5$ for $E = 0.3$, 0.5, and 1.0 in order to show that the overlap also seems to be worse for larger E. Note again the systematic shift with time. These results are consistent with those obtained through the macroscopic approach,[1, 19, 20] where a lack of clear dynamical scaling was also observed.

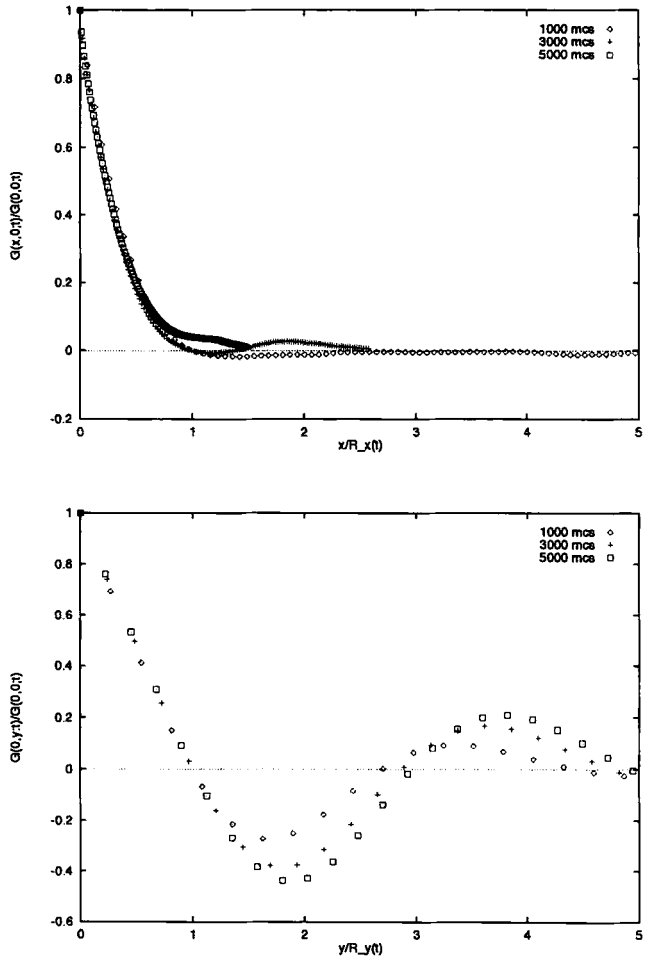

Fig. 5. Dynamical scaling with $E = 1.0$.

4.3. Reflection Asymmetry in Typical Cluster Shapes

A natural conclusion from the above analyses is that, as in the undriven case, both the microscopic and the macroscopic models appear to describe the same phenomena, though from a different perspective. However, even a casual glance at the actual configurations reveals an alarming discrepancy. At the times considered here, there is a tendency for our clusters (of particles) to take a triangular shape pointing *against* the field

(Fig. 6), i.e., "upstream." By contrast, in the macroscopic model[1] they tend to be aligned *along* the field (Fig. 7), i.e., "downstream." The latter figure was obtained using the same technique and parameters as in ref. 1 (except for the lattice size), i.e., an Euler discretization scheme with mesh size $\delta x = 1.7$, time step $\delta t = 0.25$, and external field $E = 0.4$, on a square lattice with periodic boundary conditions. The initial conditions consisted of a locally random $\phi(\mathbf{r})$, distributed according to a Gaussian with a variance of 0.02 and an average of -0.4 (equivalent to $\rho = 0.3$) or 0 (equivalent to $\rho = 0.5$).

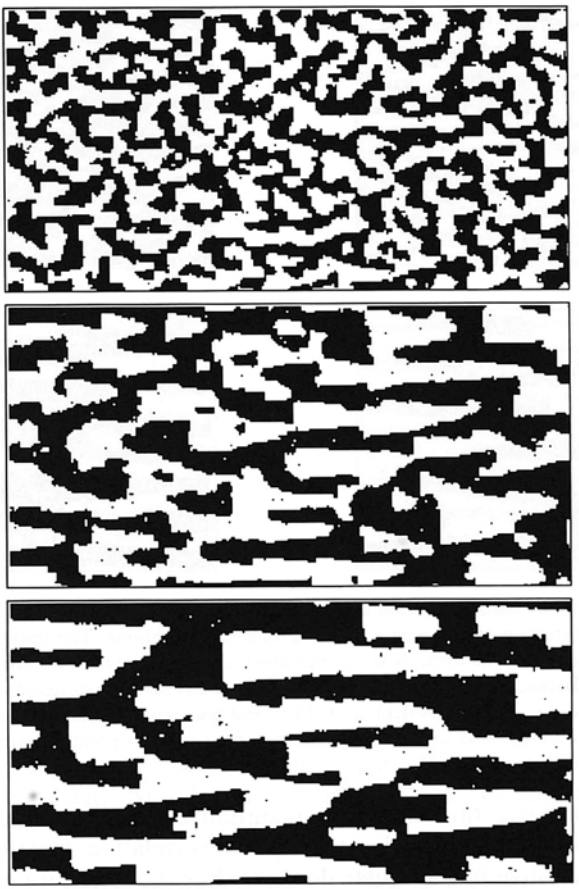

Fig. 6. Typical configurations after a quench from a disordered state obtained from Monte Carlo simulations at $t = 1000$, 5000, 10,000 MCS (top to bottom) with $E = 0.5$, $T = 0.6\, T_c$, and $\rho = 0.5$. Shown are 256×128 sections of the full 1024×512 lattice. The field points to the right, and particle clusters are in black.

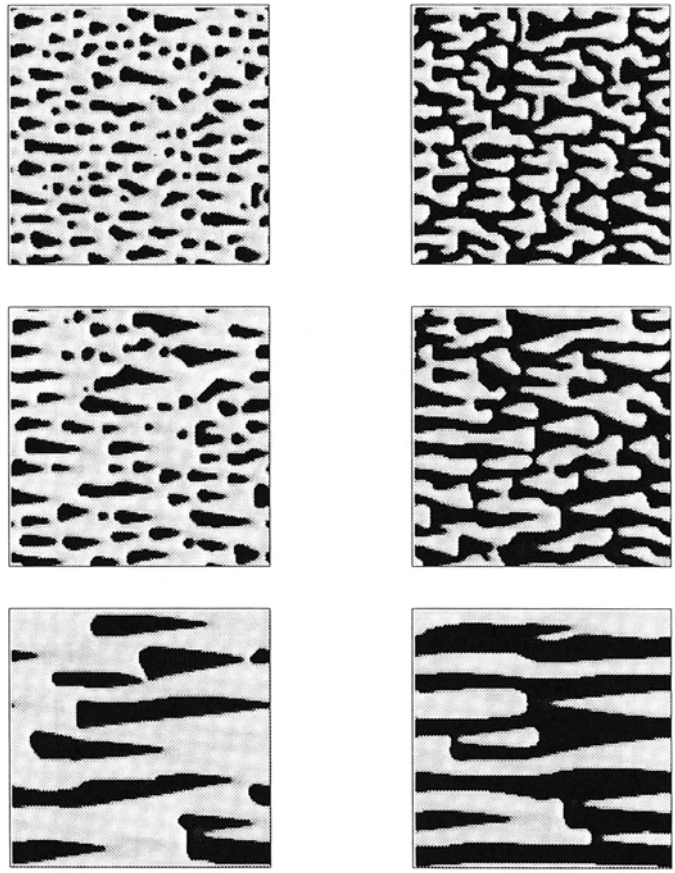

Fig. 7. Typical configurations obtained by solving the modified Cahn–Hilliard equation (13) on a 128×128 square lattice with periodic boundary conditions. The same parameters as Yeung *et al.* were used ($E = 0.4$, $dx = 1.7$, and $dt = 0.25$). The times shown are 500, 1000, and 5000 (top to bottom) in dimensionless units. The left column corresponds to an average concentration $\phi_{av} = -0.4$ (equivalent to $\rho = 0.3$) and the right column to $\phi_{av} = 0$ (equivalent to $\rho = 0.5$). The field points to the right, and dark regions correspond to particle clusters.

To investigate this difference quantitatively, we introduce an asymmetry factor, via a particular three-point correlation function[29] which should be sensitive to triangular domains. For the latter, we consider

$$G_3(x, y; t) = \sum_{x'}^{L_x} \sum_{y'}^{L_y} \eta(x', y')\, \eta(x' + x, y' + y)\, \eta(x' + x, y' - y) \qquad (19)$$

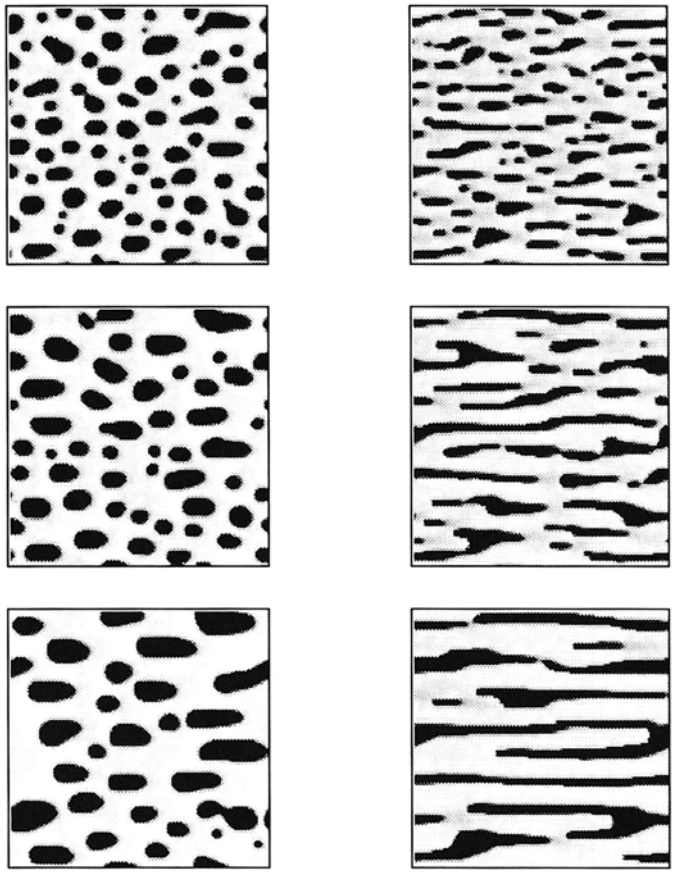

Fig. 8. Comparison between solutions of Eq. (13) (left column) with Eq. (14) (right column). For Eq. (13) the term $\mathbf{E}\cdot\nabla\phi^2$ was replaced by $\mathbf{E}\cdot\nabla\tanh(\lambda\phi^2)$. The same random initial configuration with $\phi_{\text{av}}=-0.4$ was used in both cases. The parameters $\lambda=2$, $dx=1.5$, and $dt=0.05$ were chosen. Times shown are 500, 1000, and 5000 (top to bottom). Note the apparent acceleration of the coarsening for Eq. (14).

which measures the correlation of three particles at the vertices of an isosceles triangle with base $2y$ and altitude x. Next, we define the asymmetry factor by

$$A(x, y; t)=\frac{G_3(x, y; t)-G_3(-x, y; t)}{G_3(x, y; t)+G_3(-x, y; t)} \tag{20}$$

With this definition, $A(x, y)>0(<0)$ when a configuration consists of a single triangular (say, isosceles) cluster pointing in the negative (positive)

x direction. Clearly, $A(x, y) = 0$ if the particles are distributed symmetrically relative to reflection about a vertical axis. (Remember that the system is translation invariant in the periodic box.) Such is the case when the particles are placed randomly on the lattice or if they cluster into, say, a long rectangular stripe. Hence we expect the function A to serve as a good measure for distinguishing "upstream" triangular patterns from "downstream" ones.

Though $A(x, y; t)$ is a well-defined quantity free of any empirical biases, we found that its magnitude is quite small for typical configurations.

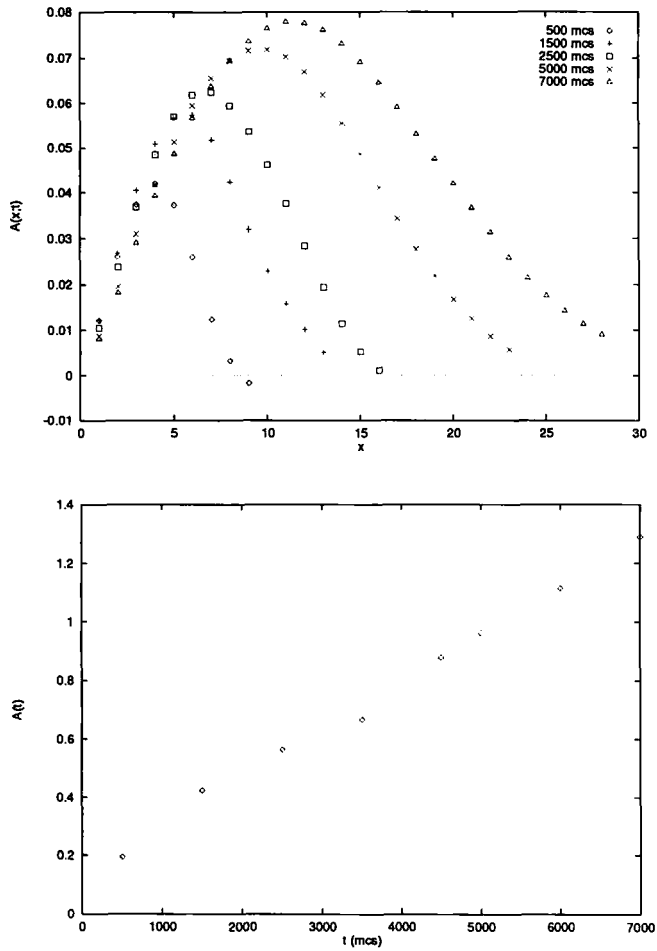

Fig. 9. Evolution of $A(x; t)$ and $A(t)$ in Monte Carlo simulations with $E = 0.3$.

Part of the reason is that typical configurations consist of many clusters, leading to cancellation effects, especially for large values of x and y. Thus, it would be helpful to consider other quantities which maximize the chances of having all three points in one cluster. This can be achieved by restricting our attention to distances within $R_x(t)$ and $R_y(t)$. Further, since we expect A to be symmetric in y, summing over y is reasonable. So, let us define two simpler measures of asymmetry

$$A(x; t) = \sum_{y=1}^{R_y(t)} A(x, y; t) \tag{21}$$

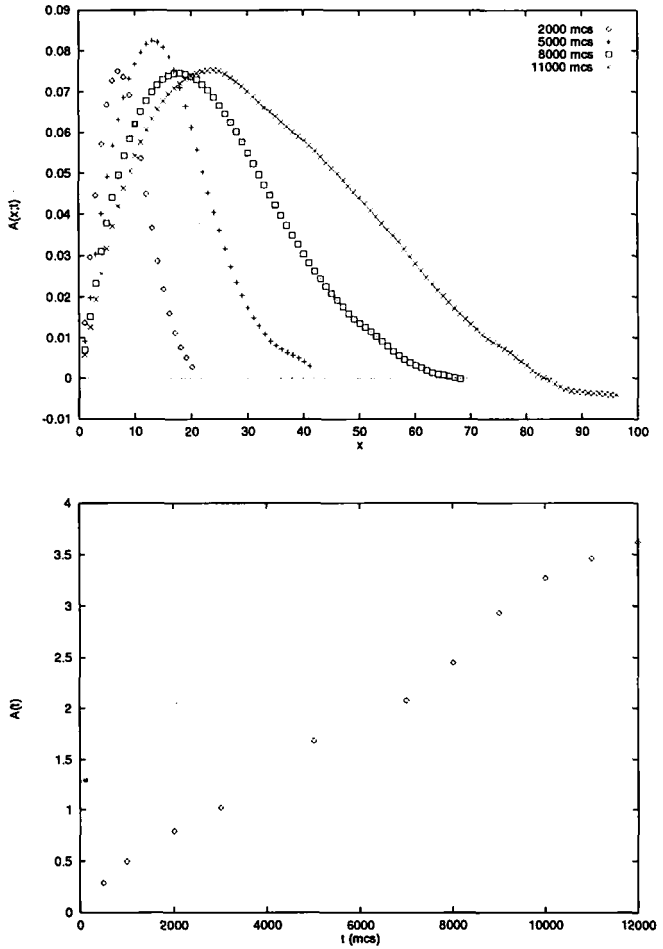

Fig. 10. Evolution of $A(x; t)$ and $A(t)$ in Monte Carlo simulations with $E = 0.5$.

and

$$A(t) = \sum_{x=1}^{2R_x(t)} A(x; t) \tag{22}$$

In the former, the upper bound $R_y(t)$[as defined after Eq. (16)] was empirically discovered to yield the largest amplitude of $A(x; t)$ for a given time t. Figures 9–11 show the results for the microscopic model with one run with $E = 0.3$, 0.5, 1.0, respectively. Though more runs would certainly

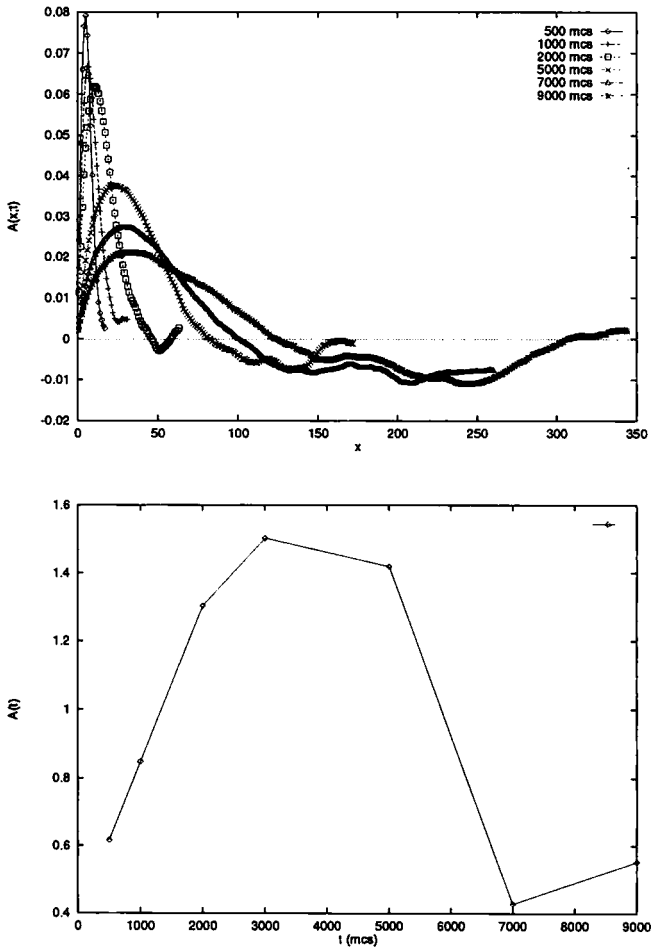

Fig. 11. Evolution of $A(x; t)$ and $A(t)$ in Monte Carlo simulations with $E = 1.0$.

be desirable, we can make some tentative conclusions based on these figures, since all functions exhibit the same general feature of rising to a maximum before dropping through zero at a larger x. It is easy to interpret such behavior: the presence of triangular patterns pointing "upstream." Further, we may define an "average size" by the peak position, which is roughly the same as $R_x(t)$. In most cases $A(x; t)$ first vanishes at a position close to $2R_x(t)$, a fact related undoubtedly to the peak positions. This is the motivation for the cutoff in the definition of $A(t)$. In Fig. 12 these are shown, corresponding to the three values of E above. Note that in the $E = 1.0$ case, this asymmetry factor reaches a maximum around 3000 MCS before falling to near zero. We may interpret this behavior as the growth of triangular patterns and their subsequent decay as the clusters begin to elongate into long, narrow stripes with little asymmetry. For the cases with smaller E, it appears that this narrow stripe regime has not been reached. This behavior is also quite reasonable, since we may expect slower rates of cluster "stretching" from smaller drives. We also observed that, at earlier times, this asymmetry factor grows faster for larger values of E. Our intuitive picture, gleaned from inspecting the time evolution of actual configurations, is that driven particles "pile up" behind a cluster, much like traffic on a multilane highway behind a blockage. Since particles can move around the obstacles, they form roughly triangular patterns against the flow. In this scenario, it is reasonable to expect the triangles to grow faster if the drive is stronger. Details aside, the A's are positive in all cases, a clear indication of triangles pointing "upstream."

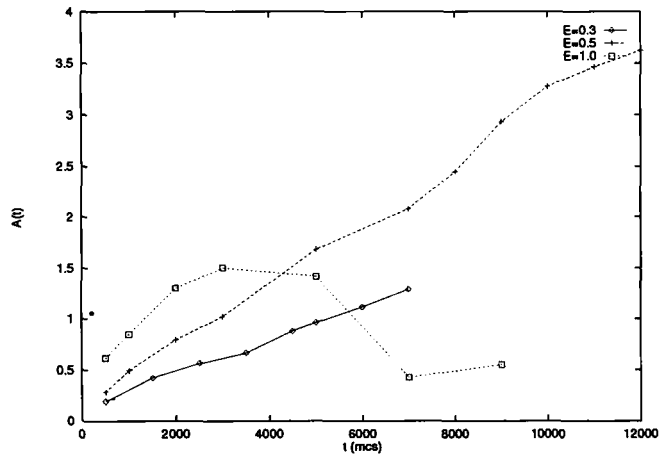

Fig. 12. Comparison of the time dependence of the asymmetric factor $A(t)$ for $E = 0.3$, 0.5, and 1.0 in the Monte Carlo simulations.

Next, we perform the same analysis on the data from the macroscopic model (see, e.g., Fig. 7). To compute the G_3 here, we replaced, at each discretized (x, y) point, positive (negative) values of $\phi(x, y; t)$ by $+1$ (0). The results for $A(x; t)$ and $A(t)$ are shown in Fig. 13. Unambiguously, both are negative, displaying similar features of rise and fall. These quantities provide a quantitative measure of the tendency of these clusters to point "downstream," in sharp contrast to the results of the microscopic model. In the remainder of this paper, we venture possible explanations of this major discrepancy.

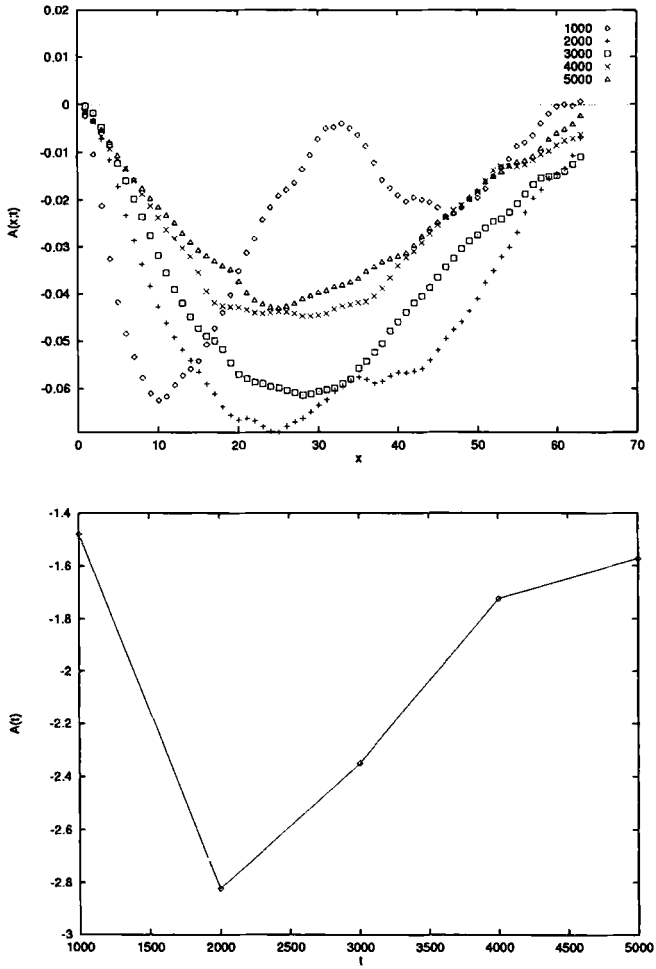

Fig. 13. Evolution of $A(x; t)$ and $A(t)$ in the macroscopic model, Eq. (13). Note the difference in sign from the results presented in Figs. 9–11.

5. CONCLUSIONS

Systems with a single conserved order parameter evolving toward thermal equilibrium following a rapid quench are quite successfully modeled by both Monte Carlo simulations of a microscopic lattice gas and numerical integration of the macroscopic Cahn–Hilliard equation. If the same system is subjected to an external drive, so that it evolves toward a *nonequilibrium steady state*, then there appear to be some similarities, as well as serious discrepancies, between the microscopic and the macroscopic descriptions.

We have performed simulations with a microscopic model[5] and repeated the studies of Yeung *et al.*[1] on a modified Cahn–Hilliard equation which is supposedly its macroscopic counterpart. Measuring the two-point correlation function and using standard definitions for "the average domain size," we find that these approaches lead to similar results. These are: (i) linear growth of clusters, with time, along the field direction, (ii) power-law growth ($t^{0.25 \pm 0.05}$) in the transverse direction, and (iii) lack of simple dynamical scaling. There is insufficient data on either model to make a quantitative comparison of these powers, so that it is premature to draw conclusions about the presence of a universality class. The lack of scaling suggests serious difficulties to obtaining a clear picture, such as in the undriven case, of the phenomenon of phase segregation in the presence of a drive.

Any hope that the micro- and macroscopic models belong to the same universality class is further dimmed by the observation that typical configurations of the two contain readily discernible triangular patterns which point in *opposite* directions. We introduced a three-point correlation function which is particularly sensitive to the presence of triangular clusters. From this, we constructed several asymmetry factors. The sign of any of these indicates the direction in which the triangles tend to point. In the regimes we have probed, these factors display similar behavior, but are opposite in sign (see Figs. 9–13)! Two alternative macroscopic approaches[19, 20] remain to be explored in detail. However, it is unlikely that they will give very different results, since they are closely related to Eqs. (13) and (12), where the nonconstant mobility stays coupled to the chemical potential term. Preliminary data on Eq. (14) show triangular clusters pointing "downstream" (see Fig. 8), albeit with a different time scale. The role of the mobility will also be explored in more detail in ref. 21, as well as the possible use of CDS to address this issue.

To reconcile these differences at the analytical level appears difficult at present. Unfortunately, we are also unable to resolve the discrepancy at the intuitive level. Above, we gave plausible arguments for "upstream"-pointing triangles; such patterns are common experience for drivers approaching toll

plazas on a highway. Whether the mechanism for the formation of such patterns is just the Mullins–Sekerka instability,[30] as observed in a similar system by Guo and Jasnow,[31] remains to be clarified. On the other hand, Yeung *et al.* gave convincing arguments for "downstream"-pointing triangles in terms of enhanced surface currents,[1] withing the context of a driven, continuous density field. In an attempt to confront these intuitive ideas, we studied the evolution of a single solid cluster of various shapes in an otherwise empty background. The results[21] further confirm the sharp contrast, namely, "upstream" growth is essentially absent in the macroscopic model.

Of course, there are many possibilities which may account for the discrepancies. We venture just two. The most glaring differences between the two approaches is the presence of noise during the evolution. In the macroscopic approach, the only randomness is in the initial configuration. The usual argument,[11, 12] based on the assumption of a constant mobility for using the deterministic CH rather than the noisy CH–Cook[32] equation, is that thermal fluctuations should play a minor role if the system is quenched to *very low* temperatures. There, the probability of the system evolving to configurations of higher (lower) energy is essentially $0(1)$. Furthermore, it was shown in refs. 33 and 11 that the addition of noise to Eq. (9) has little effect on the results once the asymptotic regime is reached. However, for our driven lattice gas, there are weaknesses in using such an argument. First, due to the presence of the external field, there is no global Hamiltonian, so that there is no clear concept of energy. The difference with the $E=0$ case would be even sharper if we had used, say $4<(Ek_BT/J)<8$, for which a two-particle cluster will be torn apart. Second, with our choice of E, the transition rates proportional to e^{-E} are far from vanishingly small. Indeed the noise becomes important if one considers Eq. (12) (with $E=0$ and α close to 1). In this case the cluster growth behaves like $t^{1/4}$ if noise is absent, while the $t^{1/3}$ growth is restored only if it is added.[36] Therefore, we plan to include noise in a future study of the macroscopic approach. Another possible shortcoming of Eq. (13) lies in the lack of anisotropy in the diffusive terms. Without anisotropy, many of the interesting properties exhibited in the microscopic model in the homogeneous, high-temperature phase could not be accounted for (see, e.g., ref. 34). Moreover, the proper description of critical behavior relies crucially on having only the transverse "diffusion constant" or equivalently the $\nabla_\perp^2\phi$ term vanish. From this point of view, it may be argued that an extreme form of anisotropic equation such as

$$\frac{\partial\phi}{\partial t}=-\nabla_\perp^2\phi+\nabla_{||}^2\phi+\cdots \tag{23}$$

would be more appropriate for $T < T_c$. We have made several attempts at introducing anisotropy. So far, no clear conclusions can be drawn, except in the following case. Integrating Eq. (23) with extreme anisotropy, we find no discernible triangular patterns before the formation of narrow stripes. Similar behavior is also observed in Monte Carlo simulations of the lattice model provided $E > 8J/k_B T$. However, more definite statements must await quantitative measurements of growth laws and asymmetry factors. Investigations along these lines are in progress.

Our work may be placed in the general context of the following questions: Given a system with a well-defined microscopic dynamics (or Hamiltonian), is there a systematic way to derive or postulate a macroscopic description which captures the essence of the microscopic system and predicts correctly the slowly varying, large-scale properties? Recently, there have been some advances to answering this question for our driven lattice gas in the high-temperature limit.[35] Similarly, an anisotropic version of Eq. (13), with positive or some vanishing $\nabla_\perp^2 \phi$ terms, proved quite successful if T is above or near criticality.[6] In particular, this approach seems to be reasonable good for predicting the three-point correlation for $T > T_c$.[29] Therefore, it is the more puzzling that Eq. (13) fails to provide even the correct sign of the asymmetry factor here. Clearly, much work remains to be done before we can claim to have a sound understanding of the microscopic–macroscopic connection. Finally, it would be most desirable to have experimental data from physical systems which could serve to resolve the conflicts presented here.

ACKNOWLEDGMENTS

We thank G. Giacomin, D. Jasnow, Y. Oono, J. Percus, S. Puri and H. Spohn for stimulating comments. This research was supported in part by NASA Grant NAG3-1414 and NSF Grants NSF-DMR 92-13424, 94-20946, 91-19102, and 94-19393. The work of F.J.A., who thanks B. J. Alder for support, was carried out under the auspices of the Department of Energy at Lawrence Livermore National Laboratory under Contract ≠ W-7405-ENG-48.

REFERENCES

1. C. Yeung, T. Rogers, A. Hernandez-Machado, and D. Jasnow, *J. Stat. Phys.* **66**:1071 (1992); see also C. Yeung, J. L. Mozos, A. Hernandez-Machado, and D. Jasnow, *J. Stat. Phys.* **70**:1149 (1993).
2. J. D. Gunton, M. San Miguel, and P. S. Sahni, in *Phase Transitions and Critical Phenomena*, Vol. 8, C. Domb and J. L. Lebowitz, eds. (Academic Press, New York, 1983); H. Furukawa, *Adv. Phys.* **34**:703 (1985); K. Binder, *Rep. Prog. Phys.* **50**:783 (1987);

J. S. Langer, in *Solids far from Equilibrium*, C. Godreche, (ed.)(Cambridge University Press, Cambridge, 1992); A. J. Bray, *Adv. Phys.* **43**:357 (1994).
3. B. D. Gaulin, S. Spooner, and Y. Morii, *Phys. Rev. Lett.* **59**:668 (1987).
4. K. Kawasaki and T. Ohta, *PhysicaA* **118**:75 (1982).
5. S. Katz, J. L. Lebowitz, and H. Spohn, *Phys. Rev. B* **28**:1655 (1983); *J. Stat. Phys.* **34**:497 (1984).
6. B. Schmittmann and R. K. P. Zia, in *Phase Transitions and Critical Phenomena*, C. Domb and J. L. Lebowitz, eds. (Academic Press, New York, 1995).
7. J. Amar, F. E. Sullivan, and R. D. Mountain, *Phys. Rev. B* **37**:196 (1988).
8. C. Roland and M. Grant, *Phys. Rev. B* **39**:11971 (1989).
9. J. Marro, J. L. Lebowitz, and M. H. Kalos, *Phys. Rev. Lett.* **43**:282 (1979); J. L. Lebowitz, J. Marro, and M. H. Kalos, *Acta Metall* **30**:297 (1982).
10. J. W. Cahn and J. E. Hilliard, *J. Chem. Phys.* **28**:258 (1958); **31**:668 (1959); J. W. Cahn, *Acta Metall.* **9**:795 (1961); *Trans. Metall. Soc. AIME* **242**:166 (1968).
11. T. M. Rogers, K. R. Elder, and R. Desai, *Phys. Rev. B* **37**:9638 (1989).
12. A. Chakrabarti, R. Toral, and J. D. Gunton, *Phys. Rev. B* **39**:4386 (1989).
13. Y. Oono and S. Puri, *Phys. Rev. Lett.* **58**:836 (1987).
14. S. Puri and Y. Oono, *Phys. Rev. A* **38**, 434:1542 (1988).
15. A. Shinozaki and Y. Oono, *Phys. Rev. E* **48**:2622 (1993).
16. K. Kitahara, Y. Oono, and D. Jasnow, *Mod. Phys. Lett. B* **2**:765 (1988).
17. J. S. Langer, N. Bar-On, and H. D. Miller, *Phys. Rev. A* **11**:1417 (1975).
18. K. Kitahara and M. Imada, *Prog. Theor. Phys. Suppl.* **64**:65 (1978).
19. S. Puri, K. Binder, and S. Dattagupta, *Phys. Rev. B* **46**:98 (1992).
20. S. Puri, N. Parekh, and S. Dattagupta, *J. Stat. Phys.* **75**:839 (1994).
21. F. J. Alexander, C. A. Laberge, J. L. Lebowitz, and R. K. P. Zia, to be published.
22. K.-T. Leung, *Phys. Rev. Lett.* **66**:453 (1991); *Int. J. Mod. Phys.* **C3**:367 (1992).
23. J. S. Wang, *J. Stat. Phys.*, to be published.
24. G. Giacomin, Ph.D. thesis, Department of Mathematics, Rutgers University; G. Giacomin and J. L. Lebowitz, to be published.
25. J. L. Valles and J. Marro, *J. Stat. Phys.* **49**:89, 121 (1987).
26. D. A. Huse, *Phys. Rev. B* **34**:7845 (1986).
27. P. Fratzl, J. L. Lebowitz, O. Penrose, and J. Amar, *Phys. Rev. B* **44**:4794 (1991).
28. P. Fratzl and J. L. Lebowitz, *Acta Metall.* **37**:3245 (1989).
29. K. Hwang, B. Schmittmann, and R. K. P. Zia, *Phys. Rev. Lett.* **67**:326 (1991); *Phys. Rev. E* **48**:800 (1993).
30. W. W. Mullins and R. F. Sekerka, *J. Appl. Phys.* **34**:323 (1963); **35**:444 (1964).
31. H. Guo and D. Jasnow, *Phys. Rev. A* **34**:5027 (1986).
32. H. E. Cook, *Acta Metall.* **18**:297 (1970).
33. S. Puri and Y. Oono, *J. Phys. A* **21**:L755–762 (1988).
34. R. K. P. Zia, K. Hwang, B. Schmittmann, and K.-T. Leung, *Physica A* **194**:183 (1993).
35. G. Eyink, J. L. Lebowitz, and H. Spohn, To be published.
36. Y. Oono and C. Yeung, Unpublished.